

# Appearance of a new phase across the $T_d$ - $1T'$ phase boundary in Weyl semimetal $\text{Mo}_{1-x}\text{W}_x\text{Te}_2$

Yu Tao,<sup>1</sup> John A. Schneeloch,<sup>1</sup> Chunruo Duan,<sup>1</sup> Masaaki Matsuda,<sup>2</sup> Sachith E. Dissanayake,<sup>2,\*</sup> Adam Aczel,<sup>2,3</sup> Jaime A. Fernandez-Baca,<sup>2</sup> and Despina Louca<sup>1,†</sup>

<sup>1</sup>*Department of Physics, University of Virginia, Charlottesville, Virginia 22904, USA*

<sup>2</sup>*Neutron Scattering Division, Oak Ridge National Laboratory, Oak Ridge, Tennessee 37831, USA*

<sup>3</sup>*Department of Physics and Astronomy, University of Tennessee, Knoxville, Tennessee 37996, USA*

Elastic neutron scattering on single crystals of  $\text{Mo}_{1-x}\text{W}_x\text{Te}_2$  reveals a new phase between the  $T_d$  and  $1T'$  phases. The new phase that we refer to as  $T_d^*$  consists of four layers rather than two in its unit cell, and is constructed by an “AABB” sequence of stacking operations rather than “AB” and “AA” for the  $1T'$  and  $T_d$  phases, respectively. The  $T_d^*$  phase emerges without disorder on warming from  $T_d$ , though further warming is accompanied by diffuse scattering indicating stacking disorder, which dissipates as the crystal warms further into  $1T'$ . On cooling, diffuse scattering is observed until  $T_d$  is reached, with a frustrated tendency toward the “AABB” stacking occurring at intermediate temperatures.

Many materials with weakly-bound layers exhibit changes in their properties when the stacking of their layers changes. For example,  $\text{MoTe}_2$  is reported to be a type-II Weyl semimetal in its orthorhombic  $T_d$  phase [1, 2] but not in its monoclinic  $1T'$  phase, even though these phases have nearly-identical layers and differ mainly in the in-plane displacements that occur when  $1T'$  is cooled into  $T_d$ . Though there is much interest in investigating Weyl semimetals, the properties of  $\text{MoTe}_2$  are not completely clear. For instance, there is much debate on the origin of the extreme magnetoresistance seen at low temperatures [3–5], the number and locations of Weyl points in the  $T_d$  phase [6], and the topological nature of observed surface Fermi arcs that are a necessary but not sufficient condition for a Weyl semimetal [7]. Structural complications are known, such as stacking disorder that arises during the transition, as seen in neutron [8] and X-ray [9] diffuse scattering; and hysteresis effects that extend far beyond the point where the bulk of the  $1T' \rightarrow T_d$  and  $T_d \rightarrow 1T'$  transitions occur, as seen in resistivity measurements along the thermal hysteresis loop [10]. The effects of complications like these are typically ignored, though one of the surface Fermi arcs has been noted to persist to  $\sim 90$  K above the transition temperature range and to have a history-dependent appearance [6]. Replacing Mo with W increases the  $T_d$ - $1T'$  transition temperature with increasing  $x$  in the formula  $\text{Mo}_{1-x}\text{W}_x\text{Te}_2$  [11, 12], but little is known of the stability of the Weyl fermions. More generally, structural phase transitions that involve in-plane translations of layers resulting from changes in temperature or pressure have been neglected compared, e.g., to those involving soft modes [13], though many materials belong to this group, including  $\text{Ta}_2\text{NiSe}_5$  [14],  $\text{In}_2\text{Se}_3$  [15, 16],  $\alpha$ - $\text{RuCl}_3$  [17],  $\text{CrX}_3$  ( $X=\text{Cl, Br, I}$ ) [18], and  $\text{MoS}_2$  [19–21]. A bet-

ter understanding of these types of transitions would not only elucidate material properties, but could lead to the discovery of new phases with new properties.

The  $T_d$  and  $1T'$  phases can be constructed from a stacking pattern of “A” and “B” operations, as shown in Fig. 1(a). The A operation maps one layer of  $T_d$  to the layer below it, so  $T_d$  can be built from repeating “AA” sequences. The B operation is A followed by a translation by  $\pm 0.15$  r.l.u., with the sign alternating layer-by-layer. Thus,  $1T'$  can be (approximately) built from repeating “AB” sequences. Diffuse scattering observed in the  $H0L$  scattering plane on cooling from  $1T'$  to  $T_d$  (in particular, the low intensity along  $(60L)$ ) is consistent with a disordered A/B stacking pattern [8]. How the stacking changes with temperature has not been closely studied, though Kim, *et al.* offered an explanation via free energy calculations for the relative stability of the  $T_d$  and  $1T'$  phases at low and high temperatures, respectively [22].

We performed elastic neutron scattering to study in detail the structural phase transition between the  $1T'$  and  $T_d$  phases in  $\text{Mo}_{1-x}\text{W}_x\text{Te}_2$ . On warming, we observed a pseudo-orthorhombic phase with a four-layer unit cell, rather than the two-layer unit cells of  $1T'$  and  $T_d$  phases. We refer to this new phase as  $T_d^*$ . The  $T_d^*$  phase is present not only in pure  $\text{MoTe}_2$  but with W-doping as well. The stacking sequence of  $T_d^*$  can be described as “AABB”, as shown in Fig. 1(a). While the  $T_d \rightarrow T_d^*$  transition is not accompanied by disorder, diffuse scattering is seen on further warming from  $T_d^*$  to  $1T'$ , and on cooling from  $1T'$  to  $T_d$ . The diffuse scattering seen from  $1T'$  to  $T_d$  suggests a frustrated tendency toward the “AABB” stacking.

Neutron scattering experiments were performed on triple axis spectrometers HB1, CG4C, and HB1A at the High Flux Isotope Reactor at Oak Ridge National Laboratory. Though all crystals are monoclinic at room temperature, for simplicity, we use the orthorhombic coordinates, with  $a \approx 6.3$  Å and  $c \approx 13.8$  Å. All measurements were done in the  $H0L$  scattering plane. The collimations for the HB1 and CG4C measurements were both  $48'-40'-S-40'-120'$ , and the collimation for HB1A was  $40'-40'-S-$

\* Present address: Duke University, Dept. of Physics, Durham, NC 27708

† Corresponding author. Email: louca@virginia.edu

40'–80'. All measurements reported in this paper were elastic, with incident neutron energies of 13.5 meV for HB1, 4.5 meV for CG4C, and 14.6 meV for HB1A.

Three  $\text{Mo}_{1-x}\text{W}_x\text{Te}_2$  crystals were measured to probe the structural phase transition. The crystals were grown in excess Te flux. Synthesis and characterization details can be found in the Supplemental Materials. The crystal “MT1” was grown without tungsten and thus has composition  $\text{MoTe}_2$ . Both the “MT2” and “MWT1” crystals were grown from ingredients that included tungsten, but from energy dispersive X-ray spectroscopy (EDS), we estimate the composition of MT2 to be  $x \lesssim 0.01$ , while for MWT1,  $x = 0.06(1)$ , where parentheses denote the uncertainty in the last digit(s). We also estimated the level of W-doping from changes in  $d$ , the out-of-plane component of the  $c$ -axis lattice constant, determined from the position of the (004) Bragg peak in longitudinal neutron scattering scans. The parameter  $d$  was determined to be 13.775(3) Å for MT1, 13.774(5) Å for MT2, and 13.8056(4) Å for MWT1. These  $d$  values suggest that MT2 is, indeed, nearly undoped, and that MWT1 has a W-fraction of  $x = 0.077(8)$  (assuming the ratio of  $x$  to changes in the  $c$ -axis lattice constant reported in Ref. [23]), which are roughly consistent with the EDS measurements. No significant Te deficiency was seen with EDS.

Figures 1(b-g) show neutron scattering intensity along  $(2, 0, L)$  as a function of temperature on cooling and warming through the hysteresis for the MT1, MT2, and MWT1 crystals. Similar patterns of scattering are seen for the three crystals. The Bragg peaks for the ordered phases are labeled in Fig. 1(d,e). At low temperatures,  $T_d$ -phase Bragg peaks at  $L = 2$  and  $L = 3$  are observed. On warming from the  $T_d$  phase, a peak appears at  $L = 2.5$  (near 260 K for MT1 and MT2, and 280 K for MWT1), indicating the onset of the  $T_d^*$  phase, which has a doubled  $c$ -axis lattice constant relative to  $T_d$  and thus can be labeled  $(205)_{T_d^*}$ . The  $\sim 20$  K higher  $T_d \rightarrow T_d^*$  transition temperature for MWT1 compared to MT1 and MT2 is consistent with the transition temperature dependence on doping reported in Ref. [12].

With additional warming, a gradual transformation into the  $1T'$  phase occurs, accompanied by diffuse scattering indicating stacking disorder. In the  $1T'$  phase, we see the  $(202)_{1T'}^{D1}$  and  $(20\bar{3})_{1T'}^{D2}$  Bragg peaks near  $L = 2.3$  and  $L = 2.7$ , respectively;  $D1$  and  $D2$  denote each of the two  $1T'$  twins. On cooling from the  $1T'$  phase, diffuse scattering is detected, and clear peaks indicating unit cell doubling along the  $c$ -axis cannot be seen. Instead, intensity remains diffuse as it shifts toward  $(2, 0, 2.5)$ , which is also shown in the individual scans in Figures S2, S3, and S4 of the Supplemental Materials. We call the region on cooling between 280 and 255 K for MT1 and MT2 (and  $\sim 20$  K higher for MWT1) the “frustrated  $T_d^*$ ” region, due to the shift in intensity toward  $(2, 0, 2.5)$ , and (to be discussed below) due to the similarity in transition onset temperatures into and away from this region as for  $T_d^*$ . For MT2, we measured through the hysteresis twice

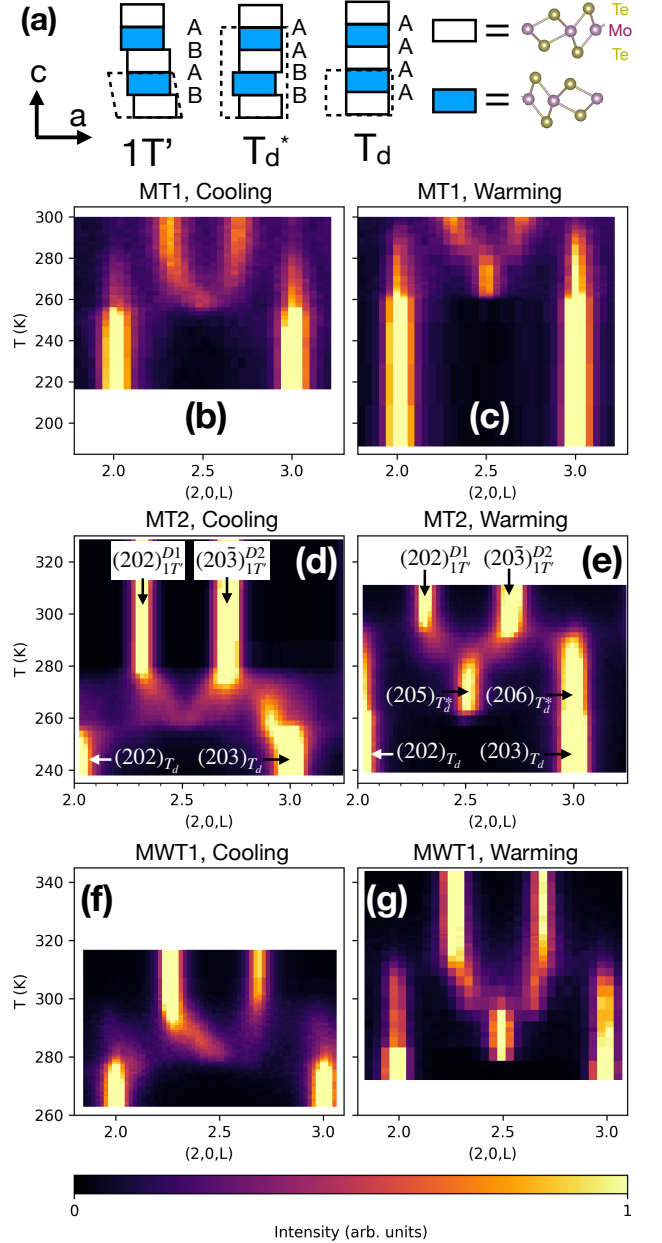


FIG. 1. (a) The stacking patterns of  $1T'$ ,  $T_d^*$ , and  $T_d$ . The dashed lines indicate the unit cell (not to scale). (b-g) Maps of the scattering intensity for (b,c) MT1, (d,e) MT2, and (f,g) MWT1 as a function of temperature along the  $(2, 0, L)$  line on cooling and warming. For MT2, Bragg peaks are labeled. “D1” and “D2” refer to the two  $1T'$  twins. Data were taken on HB1A for (b,c), HB1 for (d,e), and CG4C for (f,g).

and found the same patterns of diffuse scattering at the same temperatures along the hysteresis, suggesting that the changes in diffuse scattering through the hysteresis are reproducible.

We note that the volume fractions of the two  $1T'$  twins are generally unequal, and tend to be preserved even on

cycling through the hysteresis. From the relative intensities of the  $(202)_{1T'}$  and  $(203)_{1T'}$  peaks and the theoretical neutron scattering structure factors for these peaks, we estimate the relative volume fractions for each twin to be 67%/33% for MT1, 44%/56% for MT2, and 74%/26% for MWT1.

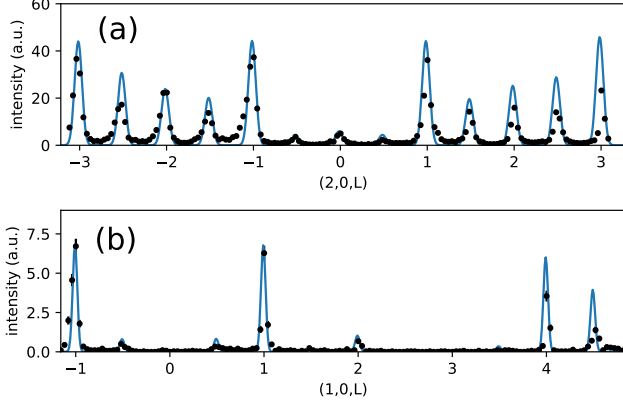


FIG. 2. Elastic neutron scattering intensity of MT2 (black markers) measured along (a)  $(2, 0, L)$  and (b)  $(1, 0, L)$ , taken in the  $T_d^*$  phase at  $\sim 266$  K. Data were taken on CG4C. Intensities in these plots are in the same arbitrary units. The blue curve is a simulation based on a model for the  $T_d^*$  phase described in the text.

We now provide a model for the  $T_d^*$  phase based on the following observations: First, the  $T_d^*$  phase appears to be orthorhombic, but has additional peaks at half-integer  $L$  relative to  $T_d$ , indicating a doubling of the unit cell normal to the layers. Second, as noted above, sequences of A/B stacking operations can be used to describe the  $1T'$  and  $T_d$  phases, and the diffuse scattering seen on cooling also appears consistent with structures built from A/B sequences [8]. There are only two A/B sequences possible for an orthorhombic phase with a four-layer unit cell: “AABB” and “ABBA”, which are twins of each other. The AABB structure is plotted in the  $a$ - $c$  plane in Fig. S7 in the Supplemental Materials. We note that this structure is incompatible with orthorhombic space groups, so it can only be pseudo-orthorhombic. Our measurements were all taken in the  $(H0L)$  plane and thus were not sensitive to position along the  $b$ -direction; thus, we cannot yet determine whether  $T_d^*$  is centrosymmetric. However, if our model is approximately correct, the  $a$ - $c$  plane positions may have inversion symmetry centers within the layers between A- and B-boundaries (as seen in Fig. S7), assuming that the  $b$ -axis positions have the same relative  $b/2$  locations as in  $T_d$  and  $1T'$ .

In Fig. 2 we compare the intensity along  $(2, 0, L)$  and  $(1, 0, L)$  for the MT2 crystal in the  $T_d^*$  phase with a calculation from a model of the stacking. The fit was optimized for a  $T_d^*$  twin fraction distribution of 48%/52%. (See Supplemental Materials for mathematical details.) There is a qualitative agreement between the model and

the data, suggesting that the “AABB” sequence does indeed describe the  $T_d^*$  phase, though more data and refinement is needed to determine the atomic coordinates more precisely. We note that in MWT1, the  $(205)_{T_d^*}$  Bragg peak is substantially more intense relative to neighboring peaks than in MT2, as can be seen from Fig. S4 in the Supplemental Materials. This difference in  $(205)_{T_d^*}$  intensity implies that the  $T_d^*$  twin fraction distribution, which is close to 50%/50% in MT2, differs substantially from 50%/50% in MWT1.

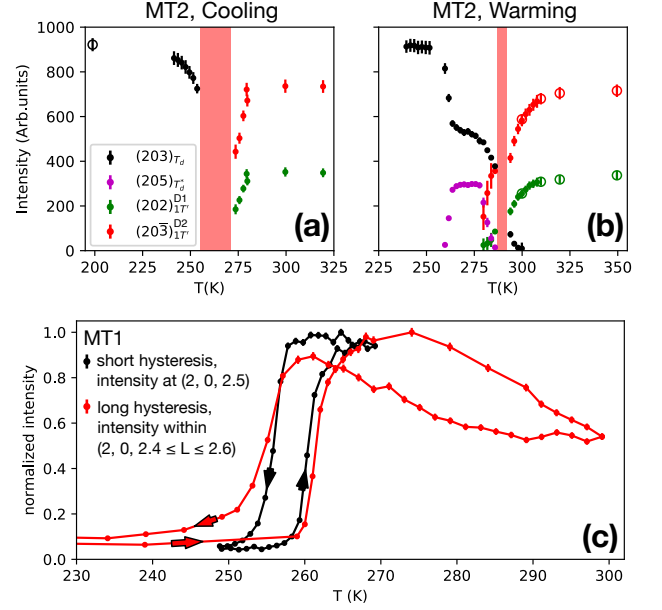


FIG. 3. (a,b) The intensity of Bragg peaks for each phase is plotted as a function of temperature on warming and cooling for MT2. The intensity is obtained from fits of individual scans of intensity vs.  $(2, 0, L)$ . The vertical red bands denote regions where fitting could not be achieved. Closed symbols denote fits to the same hysteresis loop (with cooling data measured before warming). Open symbols denote fits to data from a previous hysteresis loop. (c) Plots of intensity near  $(2, 0, 2.5)$  through two different hysteresis loops for the MT1 crystal. Both curves are normalized to their largest values. For the black curve, intensity was measured at  $(2, 0, 2.5)$  as the crystal was heated from 249 K to 269 K, then cooled to 249 K. For the red curve, intensities along  $(2, 0, L)$  (from the same data used for Fig. 1(b,c)) were averaged within  $2.4 \leq L \leq 2.6$  as the crystal was heated from 200 K to 300 K, then cooled down to 215 K.

For a closer look at how the transition proceeds, in Fig. 3(a,b) we plot several Bragg peak intensities as a function of temperature. The integrated intensities were obtained from fits of peaks present in intensity vs.  $(2, 0, L)$  scans; these data were the same as those shown in Figures 1(d) and 1(e). As we cool or warm to the extremes of the temperature range, there is a gradual increase in the intensity of the  $T_d$  and  $1T'$  peaks. This increase occurs along with a decrease in diffuse scattering, as seen in Fig. S6 in the

Supplemental Materials. However, the diffuse scattering at the temperature extremes of our measurements never completely disappeared. This lingering diffuse scattering is probably related to the long residual hysteresis commonly observed in resistivity measurements (e.g., Ref. [24]). We will argue below that the diffuse scattering present near the temperature extremes is likely due to twin domain boundaries.

In contrast, as we cool or warm away from the extremes, the intensities of the  $1T'$  and  $T_d$  peaks in Fig. 3(a) and 3(b) stay constant until a sudden change occurs, such as the decrease in the  $1T'$  peaks on cooling below 280 K or in the  $T_d$  peak on warming above 260 K. These sudden changes may correspond to kinks seen in resistivity hysteresis curves (e.g., in Ref. [24]). The drop in the  $1T'$  peak intensities near 280 K on cooling coincides with the drop in the  $(205)_{T_d^*}$  peak intensity on warming around 280 K, suggesting that 280 K marks a boundary between interactions tending to favor the  $1T'$  phase vs. the  $T_d^*$  phase, even if the longer-range stacking is different in each case.

In Fig. 3(c), we show intensity near  $(2, 0, 2.5)$  as the MT1 crystal was cycled through two hysteresis curves, both beginning on warming from the  $T_d$  phase. In the black curve, the intensity increases on heating due to the onset of the  $T_d^*$  phase peak at  $(2, 0, 2.5)$ , then decreases with a hysteresis of  $\sim 5$  K as the  $T_d^*$  phase reverts back to the  $T_d$  phase. Similar data on MWT1 (see Fig. S5 in the Supplemental Materials) show that diffuse scattering remains absent on cooling from  $T_d^*$  to  $T_d$ ; thus, both  $T_d \rightarrow T_d^*$  and  $T_d^* \rightarrow T_d$  appear to proceed without disorder. The red curve follows a larger hysteresis and shows intensity averaged within  $2.4 \leq L \leq 2.6$ . The initial increase in the red curve's intensity is due to the increase in the  $(205)_{T_d^*}$  peak intensity, but the rest of the hysteresis curve includes intensity from diffuse scattering present on further warming and subsequent cooling (as seen in Fig. 1(b) and 1(c)). Strikingly, for both hysteresis loops we see an abrupt drop in intensity on cooling at the same temperature, around 255 K, despite one loop corresponding to a system with substantial disorder, while the other loop corresponds to the  $T_d^* \rightarrow T_d$  transition proceeding without disorder.

We now discuss the transitions between  $T_d$ ,  $T_d^*$ , and  $1T'$  in terms of how short- and long-range effective interlayer interactions behave as a function of temperature. First, we propose that it is primarily the short-range effective interlayer interactions that determine the transition onset temperatures between the different phases. For example, in Fig. 3(c), whether we cool from the disordered frustrated  $T_d^*$  region or from the ordered  $T_d^*$  phase, the onset of the transition to  $T_d$  (as determined from the intensity near  $(2, 0, 2.5)$ ) occurs around 255 K. We consider the possibility that a frustrated  $T_d^*$  state has AABB-like regions embedded in an overall disordered pattern, in contrast to the ordered AABB structure of  $T_d^*$ . If short-range interlayer interactions dominate, then the temperature of the onset to  $T_d$  would be determined

by the temperature where a short-range AAAA-stacking is preferred over AABB, and would be similar regardless of disorder in the long-range stacking. If longer-range interactions contributed significantly to the free energy, then we would expect the onset temperatures to differ since the longer-range interactions would include the disordered environment to a greater degree. The similarity of onset temperatures when cooling from the frustrated  $T_d^*$  or ordered  $T_d^*$  structures thus suggests that short-range interactions are dominant.

Longer-range interlayer interactions, however, may govern the gradual increase in Bragg peak intensities (and decrease in diffuse scattering intensity) seen on warming into  $1T'$  or cooling into  $T_d$ . We propose that the residual diffuse scattering in these regimes is due to  $T_d$ -phase or  $1T'$ -phase twin boundaries. If so, individual  $A \rightarrow B$  or  $B \rightarrow A$  transitions at the boundary would not change the short-range environment, but just move the twin boundary. Thus, only longer-range effective interlayer interactions would contribute, and we speculate that they would gradually favor purer  $T_d$  or  $1T'$  phases on warming or cooling toward the temperature extremes.

Many studies on  $\text{MoTe}_2$  should be re-examined in light of the existence of the  $T_d^*$  phase. For instance, second harmonic generation (SHG) intensity measurements on  $\text{MoTe}_2$ , expected to be zero for inversion symmetry and nonzero otherwise, show abrupt (within  $< 4$  K) changes on both heating and cooling through the hysteresis loop [25]. Since the transition to  $1T'$  occurs gradually, and since  $T_d^*$  might be centrosymmetric, we suggest that the abrupt warming transition seen in SHG may be due to the  $T_d \rightarrow T_d^*$  rather than  $T_d \rightarrow 1T'$  transition. The abrupt transition on cooling is harder to explain, but it is possible that the SHG transition corresponds to the onset to  $T_d$ , and that the  $1T'$  to frustrated  $T_d^*$  transition preserves inversion symmetry, even if the transition is diffuse. Our findings may also inform proposed applications, such as the photoinduced ultrafast topological switch in Ref. [26]; since the  $T_d \rightarrow T_d^* \rightarrow T_d$  transition occurs without disorder and with only a  $\sim 5$  K hysteresis, if  $T_d^*$  is centrosymmetric, a topological switch might more efficiently use  $T_d^*$  rather than  $1T'$ .

Finally, we note that many other materials with interesting properties have sliding-layer structural phase transitions, and an improved understanding of how these phases arise may help in predicting new structures based on new stacking patterns, as well as better understanding of the properties of existing materials. Materials whose layers are weakly bound to each other and shift in-plane with pressure and/or temperature include  $\text{ReS}_2$  [27] and  $\text{ReSe}_2$  [28], which are of interest, in part, for having a direct band gap even in bulk samples;  $\text{Ta}_2\text{NiSe}_5$  [14], reported to be an excitonic insulator;  $\text{In}_2\text{Se}_3$  [15, 16], of interest as a thermoelectric material and for phase-change random access memory;  $\alpha\text{-RuCl}_3$  [17], a candidate for hosting Kitaev magnetism;  $\text{CrX}_3$  ( $X = \text{Cl, Br, I}$ ) [18], of interest for spintronics applications; and  $\text{MoS}_2$  [19–21], of interest for optoelectronics, electronic applications, etc.

Certain types of structural phase transitions have been much studied, such as those describable by soft mode theory [13], but sliding-layer structural phase transitions also deserve attention. As we have shown, a simple system of layers with a choice of two stacking operations, where the effective interlayer interactions change with temperature, can have surprisingly complex behavior.

In conclusion, elastic neutron scattering showed, for the first time, an intermediate phase in the  $T_d$  to  $1T'$  transition in  $\text{Mo}_{1-x}\text{W}_x\text{Te}_2$ . On warming from the orthorhombic  $T_d$ , the pseudo-orthorhombic  $T_d^*$  arises without diffuse scattering and corresponds to an “AABB” sequence of stacking operations, with a unit cell consisting of four layers rather than two. Diffuse scattering is present on further warming from  $T_d^*$  to  $1T'$ , and on

cooling from  $1T'$  to  $T_d$ . A frustrated tendency toward the “AABB” stacking is seen on cooling. These findings should clarify the interpretation of measurements taken across the  $T_d$ – $1T'$  transition and help answer questions related to topological properties and  $\text{MoTe}_2$ .

## ACKNOWLEDGEMENTS

This work has been supported by the Department of Energy, Grant number DE-FG02-01ER45927. A portion of this research used resources at the High Flux Isotope Reactor, which is a DOE Office of Science User Facility operated by Oak Ridge National Laboratory.

- 
- [1] Y. Sun, S.-C. Wu, M. N. Ali, C. Felser, and B. Yan, *Physical Review B* **92**, 161107 (2015).
  - [2] K. Deng, G. Wan, P. Deng, K. Zhang, S. Ding, E. Wang, M. Yan, H. Huang, H. Zhang, Z. Xu, *et al.*, *Nature Physics* **12**, 1105 (2016).
  - [3] D. Rhodes, R. Schnemann, N. Aryal, Q. Zhou, Q. R. Zhang, E. Kampert, Y.-C. Chiu, Y. Lai, Y. Shimura, G. T. McCandless, J. Y. Chan, D. W. Paley, J. Lee, A. D. Finke, J. P. C. Ruff, S. Das, E. Manousakis, and L. Balicas, *Physical Review B* **96**, 165134 (2017).
  - [4] Q. Zhou, D. Rhodes, Q. R. Zhang, S. Tang, R. Schnemann, and L. Balicas, *Physical Review B* **94**, 121101 (2016).
  - [5] S. Thirupathaiah, R. Jha, B. Pal, J. S. Matias, P. K. Das, P. K. Sivakumar, I. Vobornik, N. C. Plumb, M. Shi, R. A. Ribeiro, and D. D. Sarma, *Physical Review B* **95**, 241105 (2017).
  - [6] A. P. Weber, P. Rmann, N. Xu, S. Muff, M. Fanciulli, A. Magrez, P. Bugnon, H. Berger, N. C. Plumb, M. Shi, S. Blgel, P. Mavropoulos, and J. H. Dil, *Physical Review Letters* **121**, 156401 (2018).
  - [7] N. Xu, Z. Wang, A. Magrez, P. Bugnon, H. Berger, C. Matt, V. Strocov, N. Plumb, M. Radovic, E. Pomjakushina, K. Conder, J. Dil, J. Mesot, R. Yu, H. Ding, and M. Shi, *Physical Review Letters* **121**, 136401 (2018).
  - [8] J. A. Schneeloch, C. Duan, X. Wang, J. Liu, J. Yang, and D. Louca, arXiv:1808.05981 [cond-mat] (2018), arXiv: 1808.05981.
  - [9] R. Clarke, E. Marseglia, and H. Hughes, *Philosophical Magazine B* **38**, 121 (1978).
  - [10] T. Zandt, H. Dwelk, C. Janowitz, and R. Manzke, *Journal of Alloys and Compounds Proceedings of the 15th International Conference on Solid Compounds of Transition Elements*, **442**, 216 (2007).
  - [11] Y.-Y. Lv, L. Cao, X. Li, B.-B. Zhang, K. Wang, B. Pang, L. Ma, D. Lin, S.-H. Yao, J. Zhou, *et al.*, *Scientific reports* **7**, 44587 (2017).
  - [12] X.-J. Yan, Y.-Y. Lv, L. Li, X. Li, S.-H. Yao, Y.-B. Chen, X.-P. Liu, H. Lu, M.-H. Lu, and Y.-F. Chen, *Applied Physics Letters* **110**, 211904 (2017).
  - [13] R. A. Cowley and S. M. Shapiro, *Journal of the Physical Society of Japan* **75**, 111001 (2006).
  - [14] A. Nakano, K. Sugawara, S. Tamura, N. Katayama, K. Matsubayashi, T. Okada, Y. Uwatoko, K. Mu-  
nakata, A. Nakao, H. Sagayama, R. Kumai, K. Sugimoto, N. Maejima, A. Machida, T. Watanuki, and H. Sawa, *IUCrJ* **5** (2018), 10.1107/S2052252517018334.
  - [15] F. Ke, C. Liu, Y. Gao, J. Zhang, D. Tan, Y. Han, Y. Ma, J. Shu, W. Yang, B. Chen, H.-K. Mao, X.-J. Chen, and C. Gao, *Applied Physics Letters* **104**, 212102 (2014).
  - [16] J. Zhao and L. Yang, *The Journal of Physical Chemistry C* **118**, 5445 (2014).
  - [17] A. Glamazda, P. Lemmens, S.-H. Do, Y. S. Kwon, and K.-Y. Choi, *Physical Review B* **95**, 174429 (2017).
  - [18] M. A. McGuire, H. Dixit, V. R. Cooper, and B. C. Sales, *Chemistry of Materials* **27**, 612 (2015).
  - [19] L. Hromádov, R. Martoňk, and E. Tosatti, *Physical Review B* **87**, 144105 (2013).
  - [20] Z.-H. Chi, X.-M. Zhao, H. Zhang, A. F. Goncharov, S. S. Lobanov, T. Kagayama, M. Sakata, and X.-J. Chen, *Physical Review Letters* **113**, 036802 (2014).
  - [21] A. P. Nayak, S. Bhattacharyya, J. Zhu, J. Liu, X. Wu, T. Pandey, C. Jin, A. K. Singh, D. Akinwande, and J.-F. Lin, *Nature Communications* **5**, 3731 (2014).
  - [22] H.-J. Kim, S.-H. Kang, I. Hamada, and Y.-W. Son, *Physical Review B* **95**, 180101 (2017).
  - [23] S. M. Oliver, R. Beams, S. Krylyuk, I. Kalish, A. K. Singh, A. Bruma, Francesca Tavazza, J. Joshi, I. R. Stone, S. J. Stranick, A. V. Davydov, and P. M. Vora, *2D Materials* **4**, 045008 (2017).
  - [24] T. Zandt, H. Dwelk, C. Janowitz, and R. Manzke, *Journal of alloys and compounds* **442**, 216 (2007).
  - [25] H. Sakai, K. Ikeura, M. S. Bahramy, N. Ogawa, D. Hashizume, J. Fujioka, Y. Tokura, and S. Ishiwata, *Science Advances* **2**, e1601378 (2016).
  - [26] M. Y. Zhang, Z. X. Wang, Y. N. Li, L. Y. Shi, D. Wu, T. Lin, S. J. Zhang, Y. Q. Liu, C. N. Wang, Q. M. Liu, J. Wang, T. Dong, and N. L. Wang, arXiv:1806.09075 [cond-mat] (2018), arXiv: 1806.09075.
  - [27] D. Zhou, Y. Zhou, C. Pu, X. Chen, P. Lu, X. Wang, C. An, Y. Zhou, F. Miao, C.-H. Ho, J. Sun, Z. Yang, and D. Xing, *npj Quantum Materials* **2**, 19 (2017).
  - [28] P. G. Naumov, M. A. ElGhazali, H. Mirhosseini, V. S. E. Morosan, C. Felser, and S. A. Medvedev, *Journal of Physics: Condensed Matter* **30**, 035401 (2018).